

## One-step Hydrothermal Synthesis of $\text{Li}_{1.24}\text{Mn}_{0.66}\text{Ni}_{0.1}\text{O}_2$ Cathode for Lithium-ion Batteries

Jixian Wang<sup>1</sup>, Li Wang<sup>1,3</sup>, Xiangming He<sup>1,2,\*</sup>, Jianjun Li<sup>1</sup>, Zhongjia Dai<sup>1</sup>, Jianlong Wang<sup>1</sup>

<sup>1</sup> Institute of Nuclear & New Energy Technology, Tsinghua University, Beijing 100084, PR China.

<sup>2</sup> State Key Laboratory of Automotive Safety and Energy, Tsinghua University, Beijing 100084, PR China.

<sup>3</sup> State Key Lab of New Ceramic and Fine Processing, Tsinghua University, Beijing 100084, PR China

\*E-mail: [hexm@tsinghua.edu.cn](mailto:hexm@tsinghua.edu.cn); [wang-l@tsinghua.edu.cn](mailto:wang-l@tsinghua.edu.cn)

Received: 16 July 2015 / Accepted: 19 November 2015 / Published: 1 December 2015

---

One step hydrothermal process is attempted to synthesize Li-rich layered oxide at 140 °C~180 °C. Their morphology and crystalline structure are characterized by X-ray diffraction (XRD) and scanning electron microscopy (SEM) and transmission electron microscopy (TEM). Single phase  $\text{Li}_{1.24}\text{Mn}_{0.66}\text{Ni}_{0.1}\text{O}_2$  materials with good crystallization are obtained when the temperature is 180 °C. Their average particle sizes are 70 nm with uniform distribution of elements. The  $\text{Li}_{1.24}\text{Mn}_{0.66}\text{Ni}_{0.1}\text{O}_2$  nano-particles exhibit discharge capacities of 207 mAh g<sup>-1</sup> during the first cycle at a current of 20 mA g<sup>-1</sup> between 2.5 and 4.8 V, and remained about 81.5% after 40 cycles. This hydrothermal process paves an effective way to prepare Li-rich high capacity layered oxide cathode materials for Li-ion batteries.

---

**Keywords:** Lithium-rich layered oxide, hydrothermal, nano-particles, cation disorder

### 1. INTRODUCTION

Li-ion batteries have been widely used in consumer electronic devices, energy storage system and electric vehicles [1-4]. With the rapid development of energy storage system and electric vehicles, the traditional graphite|LiCoO<sub>2</sub> battery chemistry encounters growing challenges due to its obstacles in terms of high cost, limited energy density, safety issue and cycling life [5,6]. To this end, the Li-rich manganese based oxides with a formula of  $\text{Li}[\text{Li}_{(1/3-2x/3)}\text{Mn}_{(2/3-x/3)}\text{M}_x]\text{O}_2$  (M refers to Ni, Co, Mn, etc.) have attracted great interest in recent decade because of their high energy density [7-12]. Although they are regarded as the potential candidate for the next generation cathode materials, their high reversible capacity during first cycle, voltage fading during cycling, and poor capacity retention especially at high rate make it still be a distance to the commercialization [13,14].

Generally, synthesis plays very important role on the purity, crystallization, size distribution and finally the electrochemical performance of the materials[15,16]. Up to now, various approaches have been investigated to prepare Li-rich manganese based oxides, such as sol-gel methods [17,18], co-precipitation method[19,20], solid state method[21], combustion method[22], ion exchange method[23] and spray pyrolysis method[24]. Among all above routes, high temperature and long sintering time is generally necessary, which means high energy consuming and hard control on crystal size and morphology. Hydrothermal has been proven to be an effective way for preparing well distributed nanostructured materials[25,26]. Furthermore, Zheng et al[27] used hydrothermal assisted method to fabricate atomic level spatial distribution Li-rich manganese based material, which presented much better capacity retention and smaller voltage fade as compared to those prepared by sol-gel and co-precipitation methods.

Here, a facile one-step hydrothermal is employed to prepared Li-rich manganese material with composition of  $\text{Li}_{1.24}\text{Mn}_{0.66}\text{Ni}_{0.1}\text{O}_2$  in short time, neither precursors nor subsequent high temperature calcinations are introduced in this preparation. The influence of reaction temperature, reaction time, and concentration of LiOH solution on the purity, crystallization and size distribution of the products are studied systematically. Besides, physical, chemical, and electrochemical properties of the  $\text{Li}_{1.24}\text{Mn}_{0.66}\text{Ni}_{0.1}\text{O}_2$  nano-particles were investigated to explore the potential of its applications in lithium ion battery.

## 2. EXPERIMENTAL SECTION

### 2.1. Preparation of $\text{Li}_{1.24}\text{Mn}_{0.66}\text{Ni}_{0.1}\text{O}_2$ nano particles

$\text{Li}_{1.24}\text{Mn}_{0.66}\text{Ni}_{0.1}\text{O}_2$  nano-particles were synthesized by a facile one step hydrothermal method. First, stoichiometric ratio of  $\text{Mn}(\text{CH}_3\text{COO})_2 \cdot 4\text{H}_2\text{O}$ ,  $\text{Ni}(\text{CH}_3\text{COO})_2 \cdot 4\text{H}_2\text{O}$  and a certain amount of  $(\text{NH}_4)_2\text{S}_2\text{O}_8$  were dissolved in 10ml deionized water for 30 min to form solution A, which was added dropwise in to 30 ml LiOH solution B with a concentration at 3.3M. After continuous stirring for 30 min, a dark brown suspension was obtained. Later, this suspension was transferred into a Teflon-lined stainless steel autoclave, which was closed and allowed to react at 180 °C for a given period time. After the hydrothermal reaction, the autoclave was cooled naturally to room temperature. The obtained product was first filtered and washed with 2 mol L<sup>-1</sup> LiOH solution twice, with ethanol for 3 times and dried in air at 80 °C for 10 hrs.

### 2.2 Materials characterization

The phase structure and purity of as-prepared products were examined by X-ray diffraction (Bruker D8 Advance X-ray diffractometer in a Bragg–Brentano configuration) with Cu K<sub>α</sub>1 and Cu K<sub>α</sub>2 radiation. The crystal morphology was characterized by scanning electron microscope (SEM, JSM-5600LV, JEOL) and high-resolution transmission electron microscope (TEM, H-800, Hitachi). Elemental composition (Li, Ni and Mn) of the product was measured by Inductively Coupled Plasma

Optical Emission Spectrometer (ICP-OES, IRIS Intrepid II XSP, ThermoFisher). Specific surface areas were performed with a Nitrogen adsorption instrument (Micromeritics TriStar II, Micromeritics Inc.) at 77K.

### 2.3 Electrochemical measurements

Electrochemical performances were tested using CR2032 coin-type test cells assembled in an argon-filled glove box. The cathode film was fabricated from a mixture consisting of 80wt% active material, 10 wt% acetylene black and 10wt% polytetrafluoroethene (PTFE). Then as prepared film was cut into rounded slices with a total mass loading of around  $7 \text{ mg cm}^{-2}$ . Celgard 2400 polypropylene film was used as separator; Ethylene carbonate/dimethyl carbonate/diethyl carbonate (EC:EMC:DEC=1:1:1 by volume) solution containing  $1 \text{ mol L}^{-1} \text{ LiPF}_6$  was used as electrolyte; Li foil was used as anode. The charge-discharge tests were carried out on a Land battery test system within a voltage range of 2.5- 4.8 V vs.  $\text{Li}^+/\text{Li}$  at room temperature.

## 3. RESULTS AND DISCUSSION

### 3.1 Structures and Morphologies Characterization

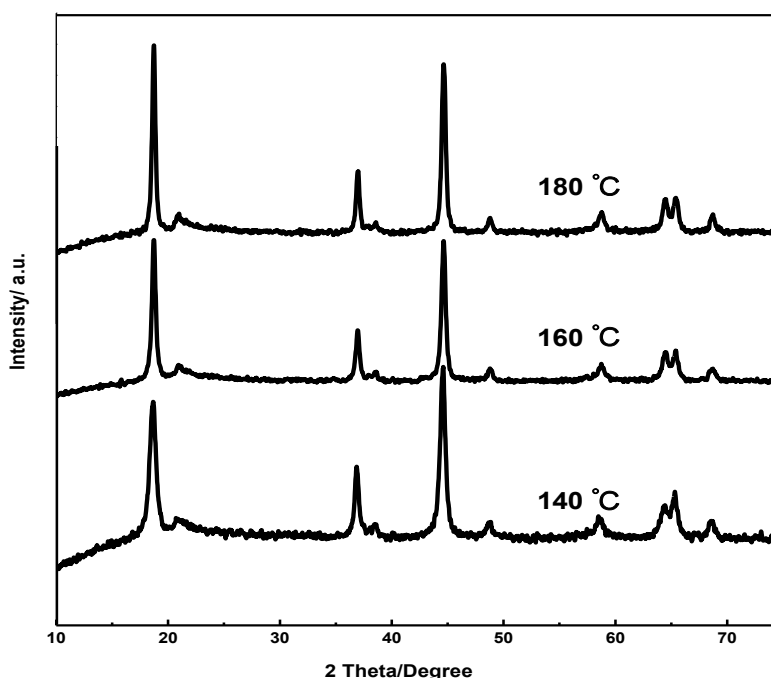


**Figure 1.** XRD patterns for the  $\text{Li}_{1.24}\text{Mn}_{0.66}\text{Ni}_{0.1}\text{O}_2$  samples prepared at 140, 160 and 180 °C, hydrothermal time: 24 h.

The XRD patterns in Fig. 1 show that the  $\text{Li}_{1.24}\text{Mn}_{0.66}\text{Ni}_{0.1}\text{O}_2$  samples prepared at 140, 160 and 180°C for 24h is single-phase material indexed well in a hexagonal  $\text{a-NaFeO}_2$  structure with R-3m

space group. Weak superstructure peaks observed around  $2\theta = 20-25^\circ$  are known to correspond to the ordering of the lithium ions and transition metal ions in the transition metal layer of the layered lattice[8,19]. Speaking of the hydrothermal product at  $140^\circ\text{C}$  for 24 h, the intensity of reflection peaks is relatively lower, demonstrating not good crystallinity as samples prepared at  $160^\circ\text{C}$  and  $180^\circ\text{C}$ . Furthermore, reflection peaks correspond to (006) and (012) directions can not be clearly distinguished, which also indicates not so good layered structure. By comparison of samples obtained at  $160^\circ\text{C}$  for 24 h with sample prepared at  $180^\circ\text{C}$  for 24h , although we can easily distinguish the reflection peak of (006) direction from (012) , with increasing hydrothermal temperature  $T_h$ , the peak intensity increases , which indicates that the crystallinity becomes better.

Moreover, the radius of  $\text{Ni}^{2+}$  (0.69 Å ) is similar to that of  $\text{Li}^+$  (0.76 Å ), cation disorder between  $\text{Ni}^{2+}$  and  $\text{Li}^+$  may hinder  $\text{Li}^+$  intercalation/deintercalation during charge/discharge. Moreover, according to Ohzuku and Makimura[28], a low ratio of peak intensity of (003) peak and (104) peak in XRD profile generally reflects poor electrochemical reactivity due to high concentration of inactive domains in layered structure. Furthermore, it's generally concluded that when  $I(003)/I(104)$  is greater than 1.1 , intact layered structure and low cation disorder are obtained[29,30]. However, according to the results of our caculation,  $I(003)/I(104)$  ratio is 0.98, much lower than 1.1, which might be correlated to irreversible capacity or poor rate capability of the material[31-33].

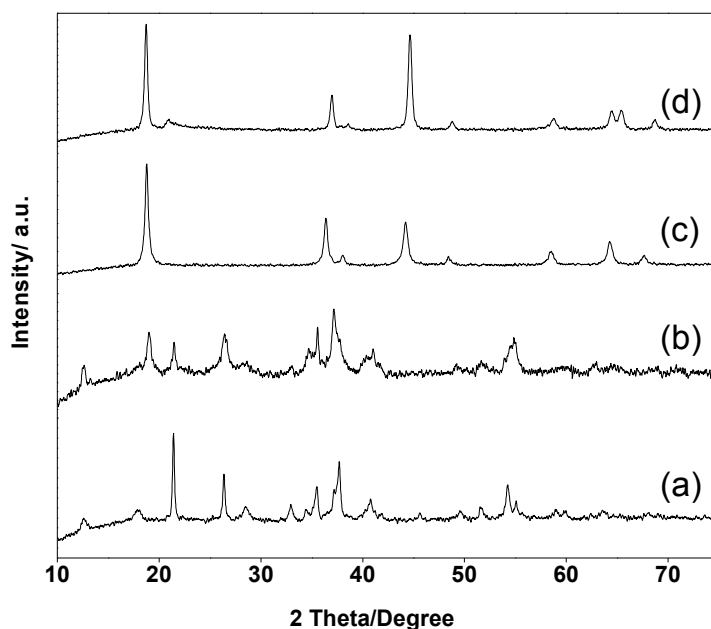


**Figure 2.** XRD patterns of the samples obtained by the hydrothermal method at  $180^\circ\text{C}$  for 24h with various  $\text{Li}/\text{M}(\text{M}=\text{Ni}+\text{Mn})$  molar ratios: (a) 2:1 (b) 4:1 (c) 7:1 (d) 10:1.

In Fig. 2, the XRD patterns of samples obtained by the hydrothermal method at  $180^\circ\text{C}$  for 24h with various  $\text{Li}/\text{M}(\text{M}=\text{Ni}+\text{Mn})$  molar ratios were given. At lower  $\text{Li}/\text{M}(\text{M}=\text{Ni}+\text{Mn})$  molar ratio, such

as 2:1 and 4:1, manganese oxide hydroxides and nickel oxide hydroxides were obtained as the main phases without any spinel and layered oxides. On the other hand, when Li/M(M=Ni+Mn) molar ratio was increased to 7:1, single phase of Li-Mn-Ni spinel was obtained. Furthermore, when we increased molar ratio of Li/M to 10:1, material indexed well in a hexagonal  $\alpha$ -NaFeO<sub>2</sub> structure with superstructure peaks observed around  $2\theta = 20$ - $25^\circ$  was obtained. This dependence of hydrothermal products on the LiOH concentration has already been reported in a previous report [34].

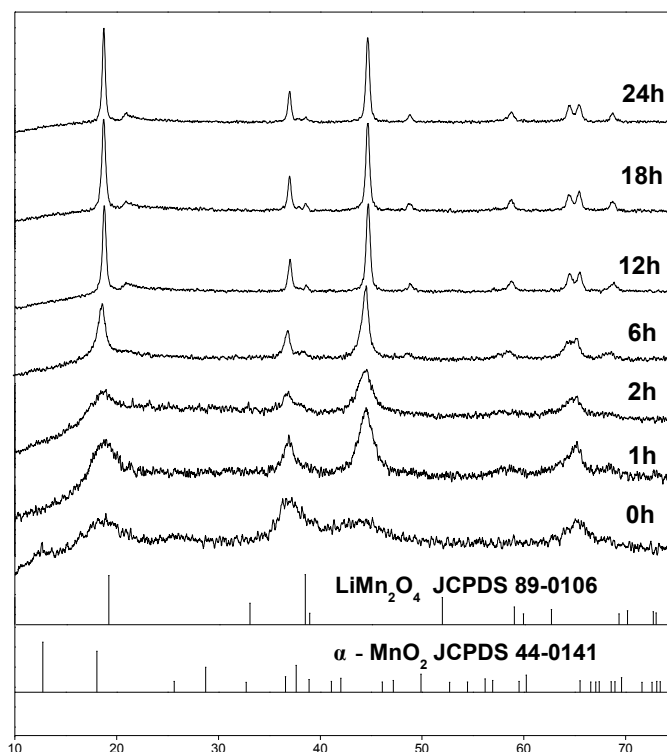


**Figure 3.** XRD patterns for the  $\text{Li}_{1.24}\text{Mn}_{0.66}\text{Ni}_{0.1}\text{O}_2$  samples prepared at  $180^\circ\text{C}$  with Li/M(M=Ni+Mn) molar ratio=10:1 for different hydrothermal time.

Fig. 3 displays the typical XRD patterns of samples obtained at  $180^\circ\text{C}$  for different hydrothermal time, which help us to study the reaction process and phase transformation. The precursor before hydrothermal reaction is probably a compound of poorly crystallized  $\alpha$ -MnO<sub>2</sub> (JCPDS 44-0141) and spinel phase Li-Ni-Mn oxides. After 1 h hydrothermal, the precursor transformed quickly into spinel structure, accompanied by the vanishment of  $\alpha$ -MnO<sub>2</sub> phase. Then, after 6 h reaction, diffraction peaks around  $2\theta = 38^\circ$  and  $65^\circ$  could be observed, which indicates the beginning of layered structure formation. Furthermore, if we prolong hydrothermal treat time to 12 h, 18 h and 24 h, all the XRD lines of the products can be indexed to the  $\alpha$ -NaFeO<sub>2</sub> layered structure. The weak superstructure reflections around  $2\theta = 20^\circ$ - $25^\circ$  indicates the ordering of the lithium ions and transition metal ions in the transition metal layer of the layered lattice[8]. ICP-OES was used to determine the elemental composition of the final product. Results shows that the experimentally observed ratio of Li:Mn:Ni in product we prepared is 1.24:0.66:0.1.

To further understand the crystallization process, we use SEM to track the morphology variation with reaction time. The precipitation before hydrothermal shows a petal like surface, which is possibly  $\alpha$ - $\text{MnO}_2$  integrating with some amorphous materials, such as Li-Ni-Mn oxides (Fig. 4a).

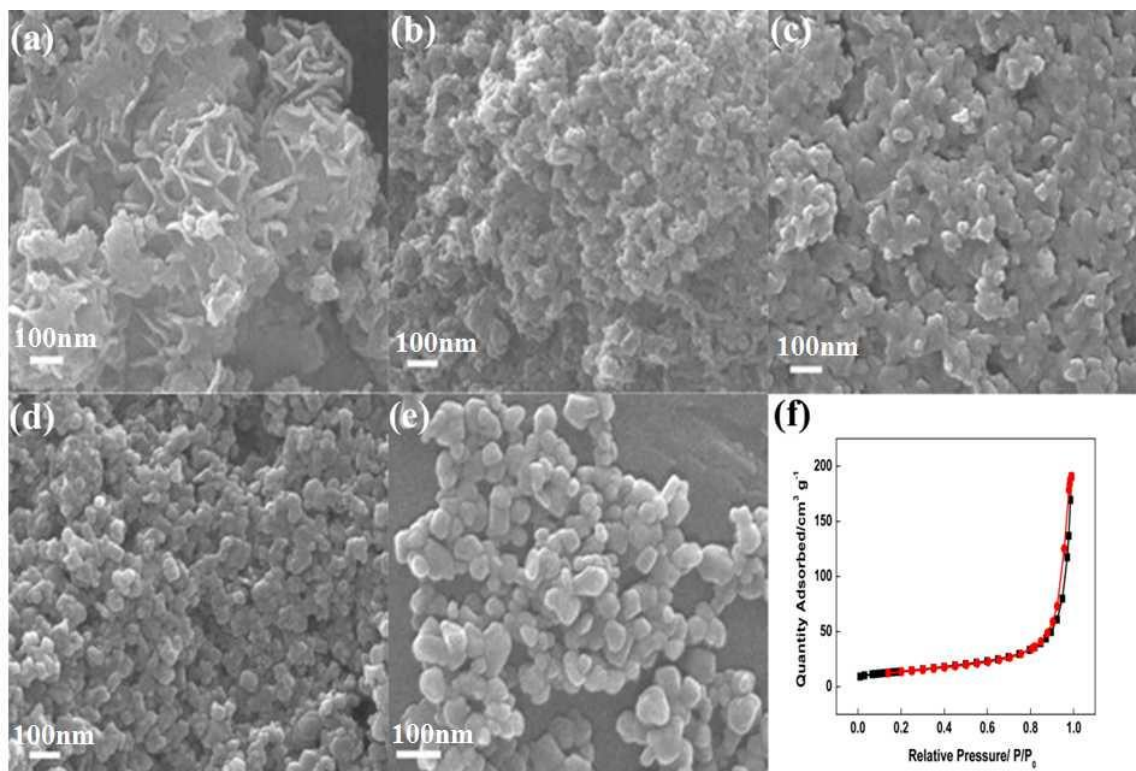


**Figure 4.** SEM images for the  $\text{Li}_{1.24}\text{Mn}_{0.66}\text{Ni}_{0.1}\text{O}_2$  samples prepared at  $180\text{ }^\circ\text{C}$  for different hydrothermal time: (a) 0 h, (b) 2 h, (c) 6 h, (d) 12 h, (e) 24 h and  $\text{N}_2$  adsorption–desorption isotherms test (f).

In the first 2 h of the hydrothermal reaction, the petal like materials are gradually disappeared and small particles with an average particle size of ca. 30 nm formed (Fig. 4b), which agrees with researches on the similar material. In detail, the petal like  $\alpha$ - $\text{MnO}_2$  can be used as precursor to prepare layered Li-Ni-Mn oxides. So in our system, with gradual disappearance of petal like  $\alpha$ - $\text{MnO}_2$ , the single phase Li-Ni-Mn-O spinel oxide formed. During the following reaction time, these nano-particles grew up to an average particle size of ca. 50 nm at 6 h (Fig. 4c) and even bigger at 12 h (Fig. 4d). Finally, after 24 h hydrothermal reaction, well-dispersed nano-particles with an average particle size of ca. 70 nm were obtained (Fig. 4e). On the basis of the morphology evolution with the reaction time, a dissolution-recrystallization mechanism [35,36] is proposed to describe the formation and growth of these  $\text{Li}_{1.24}\text{Mn}_{0.66}\text{Ni}_{0.1}\text{O}_2$  materials during hydrothermal.

The  $\text{N}_2$  adsorption–desorption measurement was carried out to characterize the surface area of the as-prepared nano-materials, as presented in Fig. 4f. The BET specific surface area was calculated to be  $49.43\text{ m}^2\text{ g}^{-1}$ , which is coincide with the particle size observed in SEM images.

### 3.2 TEM Analysis of $\text{Li}_{1.24}\text{Mn}_{0.66}\text{Ni}_{0.1}\text{O}_2$ Material

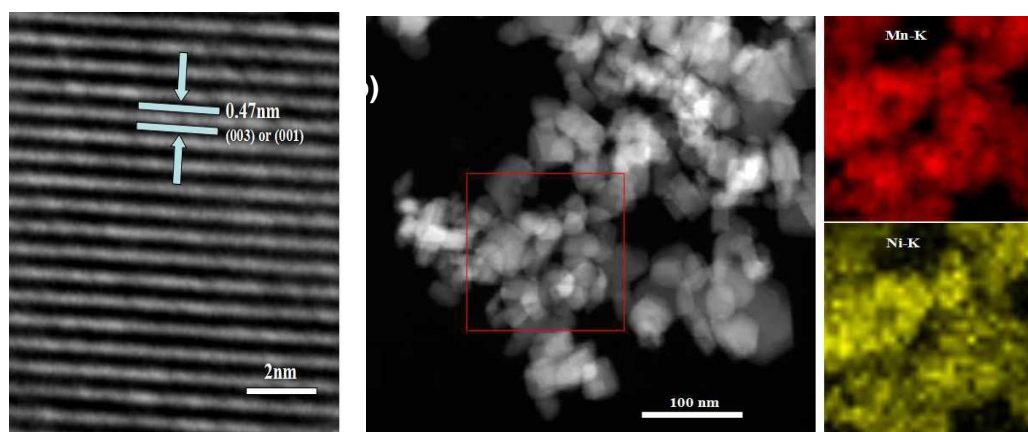


**Figure 5.** (a) HRTEM and (b) Mapping images of the  $\text{Li}_{1.24}\text{Mn}_{0.66}\text{Ni}_{0.1}\text{O}_2$  prepared at 180 °C for 24h

As shown in Fig. 5a, the fringes in HRTEM image are identified as 0.47 nm, which agrees well with the {003} or {001} lattice spacing of rhombohedral  $\text{LiMO}_2$  ( $M=\text{Mn, Ni, Co, etc.}$ ) and monoclinic  $\text{Li}_2\text{MnO}_3$ . The clear lattice-fringe observations indicated nanoparticles are with good crystallinity and no impurities exist. Besides, images of element mapping are shown in Fig. 5b, it can be observed that Mn and Ni are uniformly distributed in the sample without phase separation. This is consistent with the results obtained from X-ray diffraction patterns. Considering the results of HRTEM, it was confirmed we fabricated well distributed single phase rhombohedral  $\text{Li}_{1.24}\text{Mn}_{0.66}\text{Ni}_{0.1}\text{O}_2$  nanoparticles with good crystallinity.

### 3.3 Electrochemical performances of $\text{Li}_{1.24}\text{Mn}_{0.66}\text{Ni}_{0.1}\text{O}_2$ Material

Fig.6a depicts charge/discharge curves between 2.5 and 4.8 V for the  $\text{Li}_{1.24}\text{Mn}_{0.66}\text{Ni}_{0.1}\text{O}_2$  material prepared at 180 °C for 24 h. During the 1<sup>st</sup> charge process with current density of 20  $\text{mA g}^{-1}$ , two different regions can be observed. The first region below 4.6 V is ascribed to the oxidation of  $\text{Ni}^{2+}$  to  $\text{Ni}^{4+}$ , while the subsequent platform is assigned to the removal of  $\text{Li}_2\text{O}$ [9]. The discharge capacity in the 1<sup>st</sup> cycle is 207.4  $\text{mAh g}^{-1}$  with a coulombic efficiency of 78.2%. The poor initial efficiency is attributed to the irreversible removal of  $\text{Li}_2\text{O}$ . The cycling performance of the  $\text{Li}_{1.24}\text{Mn}_{0.66}\text{Ni}_{0.1}\text{O}_2$  material at the current density of 20  $\text{mA g}^{-1}$  is shown in Fig.6b. The capacity retention of the electrode is 81.5% after 40 cycles. The capacity fade might be attributed to following factors. One reason is the severe electrochemical decomposition of electrolyte at high potential, because of the large surface area of our material. The other reason is the unavoidable structure transformation during cycling due to thermal kinetics[13,37].

Fig.6c presents the rate capability of the prepared  $\text{Li}_{1.24}\text{Mn}_{0.66}\text{Ni}_{0.1}\text{O}_2$  material. The as mentioned structure transformation is more serious at high discharge rate. After 4 cycles discharge at 0.5C and 4 cycles at 1C, when the discharge rate is recovered to 0.1C, there is an irreversible capacity loss of 10  $\text{mAh g}^{-1}$ . As for the rate capability, this material delivers a capacity of 190  $\text{mAh g}^{-1}$  at 0.5C,

with a ratio of 91% to the capacity at 0.1C. However, the discharge capacity decreases to 97 mAh g<sup>-1</sup> when the current density is increased to 200 mA g<sup>-1</sup>, and the cycling performance deteriorate badly.

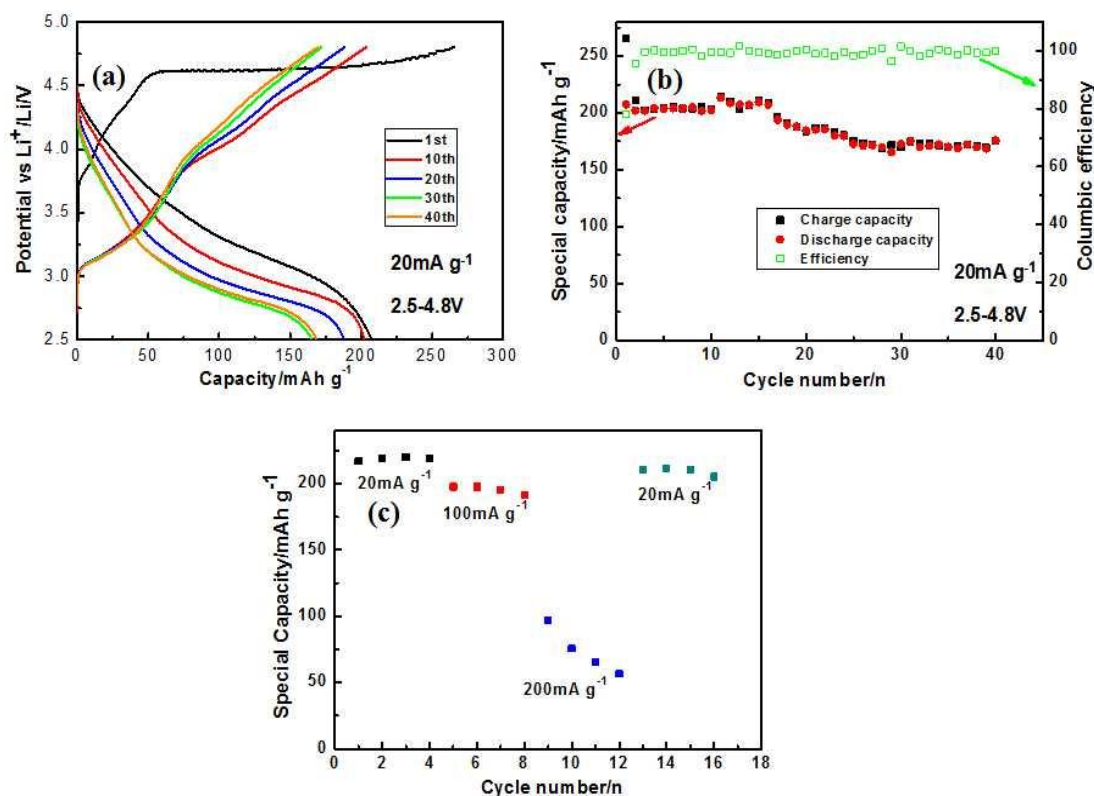


**Figure 6.** (a) Charge and discharge profiles at different cycles, (b) Cycle performance, and (c) Rate Capability of  $\text{Li}_{1.24}\text{Mn}_{0.66}\text{Ni}_{0.1}\text{O}_2$  prepared at 180 °C for 24h

As what we have discussed earlier in the XRD part, although we have fabricated single phase rhombohedral  $\text{Li}_{1.24}\text{Mn}_{0.66}\text{Ni}_{0.1}\text{O}_2$  nanoparticles with good crystallinity, according to the low  $I(003)/I(104)$  ratio, there might be high  $\text{Li}^+/\text{Ni}^+$  cation disorder, which may hinder  $\text{Li}^+$  intercalation/deintercalation during charge/discharge and cause bad electrochemical performances especially at high current density[28,32,33].

#### 4. CONCLUSION

Mono-dispersed  $\text{Li}_{1.24}\text{Mn}_{0.66}\text{Ni}_{0.1}\text{O}_2$  nano-particles can be prepared by one-step hydrothermal process. A dissolution-nucleation-growth mechanism is proposed to describe the reaction during hydrothermal, as well as formation of the crystalline nano-particles. This nano-particles can deliver a capacity of 207mAh g<sup>-1</sup> at the first cycle at a current density of 20 mA g<sup>-1</sup> in the potential window of 2.5- 4.8 V vs.  $\text{Li}^+/\text{Li}$ , and remained about 81.5% after 40 cycles. However, the rate performance at 200 mA g<sup>-1</sup> is poor and deteriorates quickly, which may due to high  $\text{Li}^+/\text{Ni}^+$  cation mixing in layered

structure. Element doping and surface modification could be efficient way to reduce such  $\text{Li}^+/\text{Ni}^+$  cation disorder, severe capacity fade at high rate. This study demonstrate that the hydrothermal process paves an effective way to prepare Li-rich high capacity layered oxide cathode materials for Li-ion batteries.

#### ACKNOWLEDGEMENT

This work is supported by the MOST (Grant No. 2013CB934000, No. 2011CB935902, No. 2014DFG71590, No. 2010DFA72760, No. 2011CB711202, No. 2013AA050903, No. 2011AA11A257 and No. 2011AA11A254), the Tsinghua University Initiative Scientific Research Program (Grant No. 2010THZ08116, No. 2011THZ08139, No. 2011THZ01004 and No. 2012THZ08129) , Beijing Municipal Program (Grant No. YETP0157, No. Z131100003413002 and No. Z131100003413001 ) , State Key Laboratory of Automotive Safety and Energy (No. ZZ2012-011) and Suzhou (Wujiang) Automotive Research Institute (Project No.2012WJ-A-01).

#### References

1. L. Wang, X. M. He, W. T. Sun, J. W. Guo, J. J. Li, J. Gao, C. Y. Jiang, *Angew. Chem. Int. Ed.* 51 (2012) 9034-9037.
2. J. M. Tarascon, M. Armand, *Nature*, 414 (2001) 359-367.
3. L. X. Yuan, Z. H. Wang, W. X. Zhang, X. L. Hu, J. T. Chen, Y. H. Huang and J. B. Goodenough, *Energy Environ. Sci.* 4 (2011) 269-284.
4. M. S. Whittingham, *Chem. Rev.*104 (2004) 4271-4301.
5. J. B. Goodenough, Y. Kim, Challenges for Rechargeable Li Batteries. *Chem.Mat.*22 (2010) 587-603.
6. M. Armand, J. M. Tarascon, *Building better batteries. Nature.* 451 (2008) 652-657.
7. C. S. Johnson, J. S. Kim, C. Lefief, N. Li, J. T. Vaughey, M. M. Thackeray, *Electrochem. Commun.* 6 (2004) 1085-1091.
8. J.S. Kim, C. S. Johnson, J. T. Vaughey, M. M. Thackeray, S. A. Hackney, W. Yoon, C. P. Grey, *Chem. Mater.*16(2004)1996-2006.
9. A. R. Armstrong, M. Holzapfel, P. Novak, C. S. Johnson, S.-H. Kang, M. M. Thackeray, P. G. Bruce, *J. Am. Chem. Soc.*128 (2006) 8694-8698.
10. S. Park, S. Kang, C. Johnson, K. Amine, and M. Thackeray, *Electrochem. Commun.* 9 (2007)262-268.
11. G. M. Koenig, I. Belharouak, H. X. Deng, Y. K. Sun and K. Amine, *Chem. Mater.* 23(2011) 1954-1963 .
12. D.Y.W. Yu, K. Yanagida, Y. Kato, H. Nakamura, *J. Electrochem.Soc.* 156(2009) A417-A424
13. Y. Wu and A. Manthiram, *Solid State Ionics.*180 (2009)50-56.
14. M. M. Thackeray, S. H. Kang, C. S. Johnson, J. T. Vaughey, R. Benedek, and S. A. Hackney, *J. Mater. Chem.* 17 (2007) 3112-3125.
15. H. W. Lee, P. Muralidharan, R. Ruffo, C. M. Mari, Y. Cui, D. K. Kim, *Nano Lett.* 10 (2010)3852-3856.
16. L. Wang, X. M. He, W. T. Sun, J. L. Wang, Y. D. Li, S. S.Fan, *Nano Lett.* 12 (2012) 5632-5636.
17. J.H. Kim, Y.K. Sun, *J. Power Sources.* 166 (2003) 119-121.
18. J. H. Kim , C. W. Park, Y. K. Sun, *Solid State Ionics.*164( 2003) 164, 43-49.
19. Z. H. Lu, L. Y. Beaulieu, R. A. Donabarger, C. L. Thomas, J. R. Danh, *J. Electrochem. Soc.*149 (2002) A778-A791.

20. J. Li, R. Klopsch, M. C. Stan, S. Nowak, M. Kunze, M. Winter, S. Passerini, *J. Power Sources*. 196 (2011) 4821-4825.
21. K. Numata, C. Sakaki, and S. Yamanaka, *Solid State Ionics*. 117 (1999) 257-263.
22. Y.J. Park, Y.S. Hong, X.L. Wu, K.S. Ryu, S.H. Chang, *J. Power Sources*. 129(2004) 288-295.
23. D. H. Kim, S. H. Kang, M. Balasubramanian, C. S. Johnson, *Electrochem. Commun.*, 12 (2010) 1618-1621.
24. M. Y. Son, S. H. Choi, J. Y. Yun, H. M. Lee, Y. C. Kang, *Int. J. Electrochem. Sci.* 8(2013) 703-719.
25. X. Wang, J. Zhuang, Q. Peng, Y. Li, *Nature*. 437 (2005) 121-124.
26. X. Wei, S. C. Zhang, L. He, G. R. Liu, P. H. Yang, *Int. J. Electrochem. Sci.* 8(2013) 1885-1894.
27. J. M. Zheng, M. Gu, A. Genc, J. Xiao, P. H. Xu, X. L. Chen, Z. H. Zhu, W. B. Zhao, L. Pullan, C. M. Wang, J. G. Zhang, *Nano Lett.* 14 (2014) 2628-2635.
28. T. Ohzuku, Y. Makimura, *Chem. Lett.* 8 (2001) 744-745.
29. J. Kim, P. Fulmer, A. Manthiram, *Mater. Res. Bull.* 34 (1999) 571-579.
30. T. Ohzuku, A. Ueda, M. Nagayama, Y. Iwakoshi, H. Komori, *Electrochim. Acta*. 38 (1993) 1159-1167.
31. K. Kang, Y. S. Meng, J. Bréger, C. P. Grey, G. Ceder, *Science*. 311(2006) 977-980.
32. S. Venkatraman, J. Choi, A. Manthiram, *Electrochem Commun.* 6(2004) 832-837.
33. S. Jouaneau, K. W. Eberman, L. J. Krause, J. R. Dahn, *J. Electrochem. Soc.* 150 (2003) A1637-A1642.
34. T. Kanasaku, K. Amezawa, N. Yamamoto, *Solid State Ionics*. 133 (2000) 51-56.
35. M. Wei, Y. Konishi, H. Zhou, H. Sugihara, and H. Arakawa, *NanoTechnology*. 16(2005) 245-249.
36. H. J. Yue, X. K. Huang, D. P. Lv, and Y. Yang, *Electrochem. Solid-State Lett.* 11(2008) A163-A166.
37. Y. J. Zhao, C. S. Zhao, Z. Q. Sun, H. L. Feng, *Acta Chim. Sin. (Engl. Ed.)* 69(2011)117-121.

© 2016 The Authors. Published by ESG ([www.electrochemsci.org](http://www.electrochemsci.org)). This article is an open access article distributed under the terms and conditions of the Creative Commons Attribution license (<http://creativecommons.org/licenses/by/4.0/>).